Spatiotemporally resolved optical emission spectroscopy and harmonic generation in Cu plasmas

M. Oujja[1], J. J. Camacho[2], M. Sanz[1], I. Lopez-Quintas[3], M. Castillejo[1], R. de Nalda[1*]

[1]*Instituto de Química Física Rocasolano, CSIC, C/ Serrano 119, 28006, Madrid, Spain*

[2]*Departamento de Química-Física Aplicada. Facultad de Ciencias, Universidad Autónoma de Madrid, Cantoblanco, 28049 Madrid, Spain*

[3]*Grupo de Investigación en Aplicaciones del Láser y Fotónica, University of Salamanca, E-37008 Salamanca, Spain*

[*]Corresponding author: r.nalda@iqfr.csic.es

Abstract

Laser-induced ablation plasmas of Cu generated by nanosecond 1064 nm pulses have been examined as media for third harmonic generation of a nanosecond driving pulse. A narrow window of ablation fluences where third harmonic generation is optimized has been identified in a region around twice the ablation threshold. A detailed analysis of the features of the Cu plasma across this critical fluence window, through spatially and temporally resolved optical emission spectroscopy, has been used to assess critical plasma parameters such as temperature, electron density, and abundance of Cu species in different ionization stages. This description has been correlated with the conditions for optimum low-order harmonic generation in the Cu plasma.

Keywords: laser ablation plasmas; optical emission spectroscopy; harmonic generation; phase matching; electron density

1. Introduction

The incidence of laser light of sufficient intensity on the surface of a solid initiates a cascade of phenomena that causes the ejection of material from the sample in the form of atoms, clusters, nanoparticles and droplets, [1], [2] often with extensive ionization. The created ablation-plasma expands in the three dimensions, with a net velocity in the direction perpendicular to the sample surface, with dynamics dominated by collisions, recombination and radiative processes [3].

A detailed understanding of laser plasmas is important for their applications in fields like laser processing of materials, [4] synthesis of thin films, [5] elemental analysis of complex samples [6] or generation of extreme ultraviolet radiation [7] or X-rays [8]. Laser plasmas are inherently transient media and present sharp gradients of measurable quantities in space and time. The understanding of the mechanisms governing plasma formation and expansion is a challenging task that requires a detailed description of the dynamics in the solid from the laser-matter interaction to the formation of the plasma, and the subsequent plasma evolution and expansion. Some of the experimental techniques employed to describe these media are time-of-flight methods, [9] interferometry and fast photography [10]. The detection of optical emissions by excited particles in the plasma is particularly suitable and informative, since it can provide information not only on the composition of the plasma but also on the electron density and temperature, [11], [12], [13] with spatial and temporal resolution.

As nonlinear optical media, laser plasmas offer interesting routes for exploration and optimization, due to their often complex composition, the presence of species that do not appear in other environments and the broad range of values that macroscopic variables like temperature or electron density can span across. A significant body of literature exists

describing harmonic generation in plasmas generated through laser ablation. Among these, some experiments have the exploited resonance enhancement of a given harmonic due to a resonance with a species present in the plasma, [14], [15] others have described harmonic generation in species like fullerenes, [16] clusters [17], [18], [19] or nanoparticles [18], [20], [21]. Additionally, the macroscopic conditions of the plasma region where harmonics are generated (temperature, gas pressure, electron density) have been shown to play a crucial role on harmonic emission [17], [22].

One of the main drivers of the studies of plasmas as nonlinear optical media has been the search for improved characteristics of harmonic emission, be it in the form of higher efficiency, higher cutoffs in high-order harmonic generation or intense generation of a given harmonic. In that arena, previous work has mainly focused on high-order harmonics generated with ultrashort near-infrared laser pulses [15], [17], [20]. However, it has been shown that the observation of harmonics from a laser plasma also constitutes a powerful diagnostic technique of the plasma itself, and can be sensitive to properties of the laser plasmas that are elusive through other techniques. This type of study has been dominated by low-order harmonic generation [14], [18], [19], [21], [23], [24]. Given that laser plasmas are media with local inversion symmetry, so that only odd harmonics can be emitted, the first orders to be observed are the third and fifth. When harmonic generation is employed as a tool to diagnose the laser plasma, it is important to design experiments that allow complete spatio-temporal exploration across broad ranges (at least millimeters in space, tens of microseconds in time). An example of this type of measurement can be found in [19], where a detailed temporal analysis of harmonic generation allowed the detection of middle-sized species in a complex fs plasma.

The crucial roles of both microscopic (i.e. the local composition of the plasma) and macroscopic (i.e. dispersion) characteristics of laser plasmas on harmonic generation

have been broadly acknowledged in previous literature [17], [25], [26], [27]. In some previous contributions by us and other authors it had been described how optical emission spectroscopy can be used for a qualitative assessment of species present in the plasma where harmonic emission takes place [19], [21], [22], [28], [29]. Also, OES assessment of the electron density in plasmas employed for harmonic generation has been reported for instance in [25], or even, in a reverse approach, harmonic generation has been employed as a measurement of electron density through OES in a quasi-phase matching configuration [30]. On the other hand, detailed analysis of optical emissions has shown to be an invaluable tool for the description of laser-induced plasmas [13], [31], [32], one that can not only provide information on a given parameter like electron density but that, particularly when performed with high spatial, temporal and spectral resolution, can yield valuable and precise information on a broad range of plasma characteristics like composition, excitation temperature, degree of ionization or plasma expansion behaviour. However, a detailed description of the features of the plasma through optical emission spectroscopy, together with the determination of their repercussions on harmonic generation, is, to our knowledge, lacking. Contributing to filling this gap constitutes the main aim of this work, where we report the results of an experiment designed to study the behavior of a laser-generated Cu plasma as a nonlinear optical medium, in a spatiotemporal region diagnosed through optical emission spectroscopy. This allows us to determine the conditions, both micro- and macroscopic, that optimize third-order harmonic generation in a laser-generated Cu plasma.

2. Materials and methods

The experimental scheme employed in this work is presented in **Figure 1**. The output of a Q-switched Nd:YAG laser (Spectra Physics, Quanta Ray Indi-HG, 1064 nm, 6 ns

pulses, 10 Hz) was used for ablation of Cu samples inside a stainless steel vacuum chamber with a base pressure of $\approx 2\times10^{-5}$ mbar. The metal samples were 2 mm thick, 10 mm diameter cylinders (Kurt J. Lesker, 99.99% purity) held onto a continuously rotating holder. The laser beam was focused onto the target surface at normal incidence using an f = 20 cm lens. The Cu sample was placed ahead of the focal plane of the ablation beam in a position where the laser spot on the surface had a slightly elliptical shape with dimensions of around 700 μm × 800 μm. We will refer to this situation as "soft focusing" geometry.

We performed two types of experiments on the Cu ablation plasmas obtained under the same conditions: detection of spontaneous emissions by optical emission spectroscopy (OES) from the excited species in the plasma and detection of the third harmonic (TH) of a second laser beam that crosses the plasma at controlled delays. In most cases the OES experiments are performed only with the pump laser pulses, while TH generation experiments require pump and probe lasers beams (see Fig. 1). It has been checked that spontaneous plasma emissions do not differ significantly when using single pulse or double pulse configuration.

For the OES measurements, the plasma emission was collected and imaged onto the entrance slit of a 0.3 m spectrograph (Bentham, TMc300, grating with 1200 lines/mm blazed at 500 nm) coupled to an intensified charge-coupled device (ICCD) camera (Andor Technology, DH501-25F-03, 1024 × 128 active pixels, 26 μm × 26 μm pixel, intensifier diameter 25 mm). The image was 2:1 magnified with a set of two lenses and rotated by 90º with a quartz Dove prism. This allowed to project the expansion axis of the plasma onto the entrance slit of the spectrograph, obtaining spatial resolution in the vertical axis of the detector and spectral resolution in the horizontal axis. We will refer to this type of measurements as 1D-1D OES (see reference [13]). In these conditions the spatial

resolution is mainly limited by pixel size, which is around 26 µm × 26 µm. The ICCD detector was temporally gated for 100 ns for the acquisition of emissions at selected delays after the ablation event. The intensity response of the detection system in the spectral region 350 - 600 nm was calibrated using a tungsten filament lamp (Osram Xenophot HLX 64640, 24 V, 150 W) (see ref. [32] for more details).

For TH measurements, a second NIR laser pulse, which will be subsequently called driving laser, was employed as the fundamental radiation for harmonic generation. It was produced by a second Q-switched Nd:YAG system (Lotis TII LS-2147, 1064 nm, 15 ns pulses, 10 Hz), which propagated across the plasma perpendicularly to the ablation laser beam and parallel to the Cu surface at a distance of approximately 1 mm. This driving beam was focused with a f = 20 cm focal length lens on the plasma expansion axis. A confocal parameter of b = 4 mm was determined from the characterization of beam geometry in the focal region. The driving laser intensity in the plasma area is estimated around 2×10^{11} W/cm^2. The delay between the two nanosecond lasers can be varied arbitrarily, since it is controlled electronically, and the resolution is only limited by their pulse width. The time resolution in detection is limited by the rise time in the ICCD, which is around 2 ns. For these measurements the Dove prism and the imaging system were removed and replaced by two dichroic mirrors enhanced for 355 nm reflectivity. For spectral dispersion, the same spectrograph described above was used, with a grating of 300 lines/mm. In these conditions the spectral resolution was around 0.25 nm.

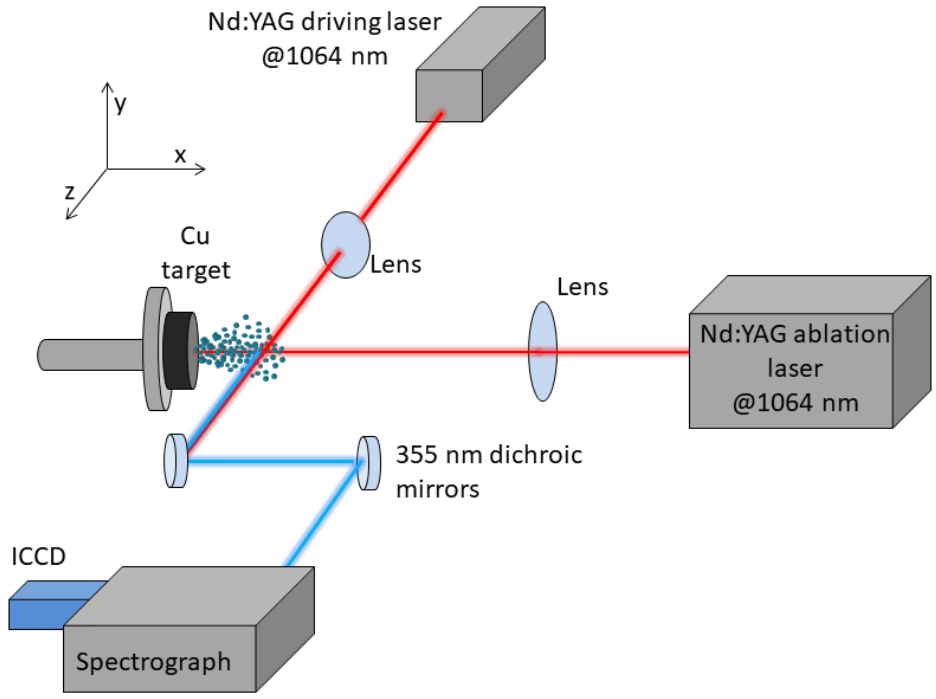

Figure 1. Experimental scheme employed for the measurement of the nonlinear optical response of the laser ablation plasma through the detection of the third harmonic of an NIR fundamental pulse propagating across the Cu plasma.

3. Results

3.1. Third-order harmonic generation

The nonlinear optical response of the ablation plasma is a rapidly varying function of the spatial and temporal coordinates, in correlation to the rapidly varying composition of neutral and ionized species present in the expanding medium. As described in previous reports, [14], [21] the intensity of the TH of the driving beam as a function of the *x* coordinate (see **Figure 1**, where *x* measures the distance to the target surface) decays rapidly, following the rapidly decaying density. For the experiments described in this work we chose 1 mm as a compromise distance that avoids irradiating the target surface with the driving beam while at the same time keeping a strong nonlinear signal. The signal intensity also depends strongly on the position of the focal plane of the driving beam with

respect to the plasma expansion axis (along the *z* direction in **Figure 1**). In this respect, for the measurements described below, we placed the focal plane of the driving beam on the axis of the expanding plasma ($z = 0$). In this spatial configuration, we measured the third harmonic of the fundamental beam as a function of the delay time with respect to the ablation event, for three different values of the laser ablation fluence on the target (2.7, 3.4 and 4.7 J/cm^2). The results of this measurement are shown in **Figure 2**. The graph shows that the main feature in the temporal response is a peak in the region of 300-500 ns and a decay for delays of 1 μs and longer. The temporal behavior of the main peak does not seem to depend strongly on the laser fluence on target, except a slight temporal displacement to longer times for the lowest fluence employed, which can only be assessed by calculating the center-of-mass of the distribution around the peak. The ratio of delay maxima for different fluences is of the order of that expected by assuming that the kinetic energy acquired by the plasma particles is linearly dependent on laser fluence, causing lower average kinetic energies for lower laser fluences, resulting in turn in longer times required to reach the interaction region. Another feature worth mentioning in the results shown in **Figure 2** is the presence of a weaker, delayed temporal component appearing in the region of 10-20 μs, mostly visible for the highest fluence employed. This late component has been described in previous works and has been attributed to the presence of a low speed component of the expanding plasma dominated by nanoparticles [18], [21]. The harmonic emission was explored for longer delays until 200 μs but no signal was observed beyond 30 μs.

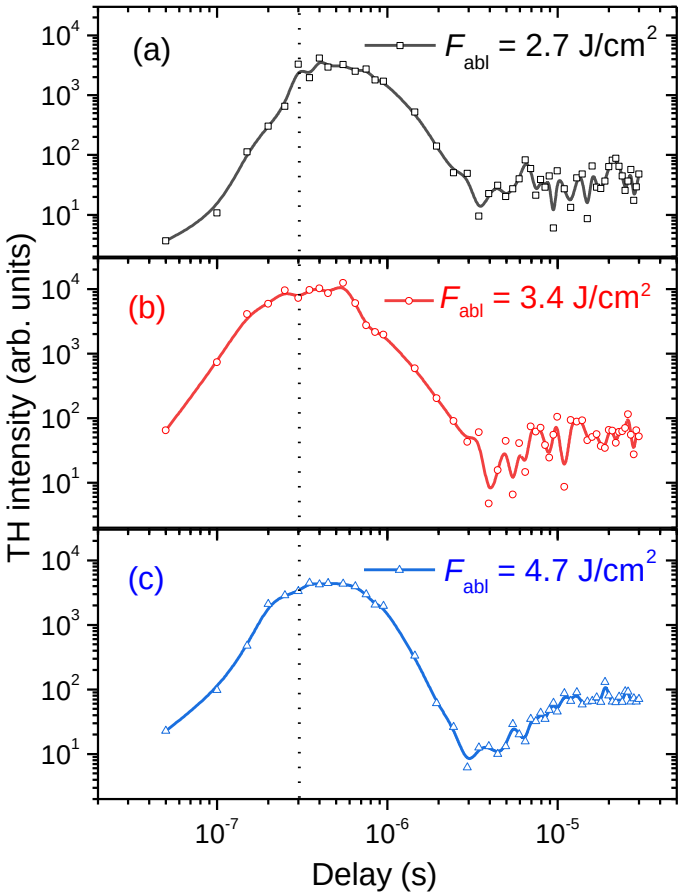

Figure 2. Intensity of the TH generated in the Cu plasma as a function of the delay time with respect to the ablation event. Note that the graph is plotted on a log-log scale. The three panels correspond to the three ablation fluence values of (a) 2.7 J/cm^2, (b) 3.4 J/cm^2 and (c) 4.7 J/cm^2 as indicated. The dotted line at 300 ns indicates the temporal delay position where subsequent measurements were acquired.

Even though the normalized temporal behavior of the early temporal component does not show important changes with laser fluence for the values employed in the above measurements, maximum TH signal levels do show a strong dependence on fluence. In order to show this, we have selected a fixed delay time of 300 ns with respect to the ablation event and measured the TH signal as a function of fluence in the 1-25 J/cm^2 range. The results are plotted in **Figure 3**, where the harmonic generation intensity is

plotted together with spontaneous emissions from the Cu plasma acquired simultaneously. The most prominent emission in this region is the Cu doublet corresponding to the decay of the outermost electron from the 4p orbital to the ground state 4s orbital, i.e. $3d^{10}\ 4p(^2P^0_{3/2}) \rightarrow 3d^{10}\ 4s(^2S_{1/2})$ and $3d^{10}\ 4p(^2P^0_{1/2}) \rightarrow 3d^{10}\ 4s(^2S_{1/2})$, emitting at 324.75 nm and 327.40 nm, respectively. The evolution of the intensity of the emission at 324.75 nm is shown in **Figure 3** (in red). For high ablation laser fluences, a weak line that can be attributed to Cu^+ in its $3d^8\ 4s^2(^1G) \rightarrow 3d^9\ 4p\ (^3F^0)$ transition is also detected at 368.66 nm; the evolution of the intensity of this line is shown on the graph (in blue). The relative intensities of the third harmonic and these two emissions are not comparable; they have been scaled so that they can be visualized on the same graph.

We shall first direct our attention to the inset of **Figure 3**, where the measurements correspond to fluences around the ablation threshold. These results provide estimates of the threshold fluence. Harmonic generation is observed at a fluence of ≈ 1.7 J/cm^2, whereas spontaneous emissions require somewhat higher fluence, in the region of ≈ 2.7 J/cm^2. It must be recalled that harmonic generation is sensitive to the presence of ground state Cu atoms, whereas spontaneous optical emissions require a certain degree of electronic excitation. The finding of a laser fluence window where only ground state atoms are produced has been described before for infrared laser ablation of metals [33], [34]. These experimental values should be compared with previously reported data and with estimations of laser ablation threshold fluence in Cu. For metals irradiated with nanosecond pulses, laser wavelength is normally not the important parameter, since there is sufficient time for heat conduction during irradiation and thus the affected layer is defined by the thermal properties of the material and the pulse duration. In this case the threshold laser fluence can be estimated from the relation[35]·[36] $F_{\mathrm{th}} = \rho\Omega\sqrt{D}\sqrt{\tau_p}$, where ρ is the density of the solid (8.96 g×cm^{-3} for Cu), Ω is the latent heat of vaporization

(4.73×10^3 J×g^{-1}), D is the heat diffusion coefficient (0.28 cm^2×s^{-1}), and τ_p is the laser pulse duration (6 ns). The heat diffusion coefficient was calculated through $D = k/(\rho C_p)$ where k (0.96 Cal × s^{-1} × cm^{-1} × K^{-1}) is the thermal conductivity and C_p (0.38 Cal×g^{-1}×ºC^{-1}) is the specific heat. From the above equation, the calculated threshold fluence of Cu for the laser used in these experiments is 1.7 J/cm^2. This is in very good agreement both with our determination based on detection of harmonic signal and with previous experimental values [37], [38]. Thus, it is worthwhile noting that the measurement of the third-order harmonic generation in laser plasmas as a function of the fluence of the ablation laser can be used as a method for the determination of the ablation threshold, due to its sensitivity to the presence of non-emitting species.

The results shown in **Figure 3** indicate that the TH signal at 300 ns delay grows very rapidly with fluence in the region 1.7-3.7 J/cm^2, with a maximum at 3.7 J/cm^2, and then decays to very low values for higher fluences. Contrarily, the intensity of the spontaneous emissions, both those attributed to neutral Cu atoms and Cu^+ ions, show a monotonous rise as a function of laser fluence.

For increasing ablation fluences up to the region of maximum harmonic emission (3.5 J/cm^2), it is clear that higher fluences imply higher number density of emitters in the interaction region, causing a higher harmonic generation intensity. Beyond this region, even though the total density is bound to increase, as is revealed by the monotonously growing signals of the spontaneous emissions, the third harmonic emission undergoes a dramatic drop. This rather counterintuitive behavior of harmonic generation efficiency as a function of laser ablation fluence has been found before [29], [39] and had been qualitatively attributed to the detrimental role of increasing electron density for phase matching.

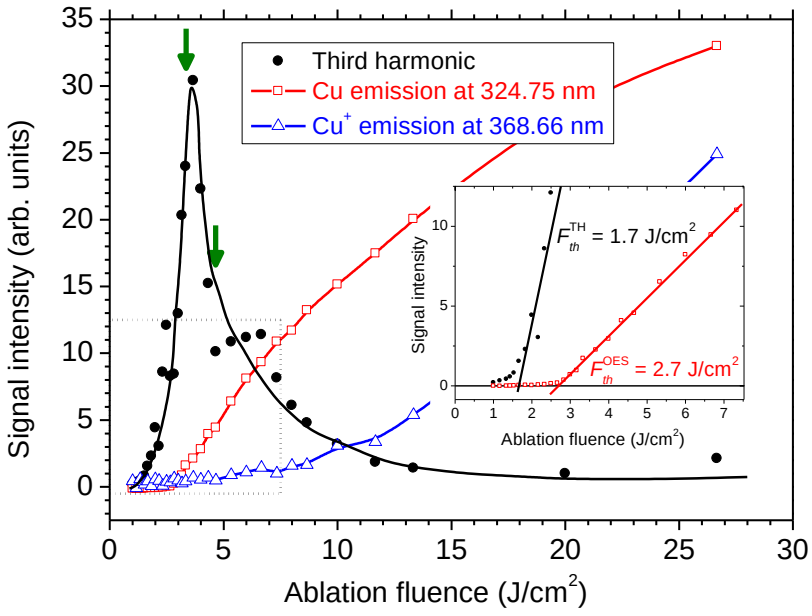

Figure 3. Intensity of the TH of the NIR fundamental laser beam generated in the Cu plasma as a function of the ablation laser fluence for a fixed delay of 300 ns (black solid circles). Spontaneous emissions from Cu (red open squares) and Cu^+ (blue open triangles) detected simultaneously are also plotted on the graph (see text for details). The inset shows a zoomed out section near the threshold laser fluence (indicated in the main graph with a dotted box) wherefrom estimates of threshold fluences are obtained. The arrows indicate the fluence values for which OES experiments were performed (see below).

These results above indicate that, within a relatively narrow interval in ablation laser fluence, from 3 to 5 J/cm^2, the characteristics of the plasma that determine the conditions for third harmonic generation undergo a profound change. This led us to pursue further exploration into the nature of the Cu laser plasmas generated in these conditions. To that end, we have performed OES experiments in the absence of the driving laser pulse at the two fluences indicated with arrows in **Figure 3** (3.4 and 4.7 J/cm^2). From this point onwards, we will call these situations *plasma 1* (3.4 J/cm^2) and *plasma 2* (4.7 J/cm^2).

3.2. Spatiotemporally resolved optical emission spectroscopy

For fluences above ≈ 2.7 J/cm^2, emissions from the plasma start to become detectable. **Figure 4** shows 1D-1D maps (on a wavelength-distance space) of OES emissions from the Cu plasma in the most informative region of 480-530 nm. The top row corresponds to data acquired for an ablation laser fluence of 3.4 J/cm^2 (*plasma 1*) and the bottom row, to 4.7 J/cm^2 (*plasma 2*). Data are shown for three selected delays with respect to the ablation event: from left to right, these are 0, 100 and 300 ns. On all panels of **Figure 4**, two horizontal lines mark the region of 0.5 - 1.0 mm distance from the target, where the interaction occurs with the driving laser in harmonic generation experiments. Integration of signals across this spatial interval leads to the emission spectra shown on top of each map. Emissions from neutral Cu are dominant for the lower fluence used at all times, in particular three well defined emissions detected at 510.55 nm, 515.32 nm and 521.82 nm corresponding to the transitions $3d^{10}4p\ (^2P°_{3/2}) \rightarrow 3d^94s^2\ (^2D_{5/2})$, $3d^{10}4d\ (^2D_{3/2}) \rightarrow 3d^{10}4p\ (^2P°_{1/2})$ and $3d^{10}4d\ (^2D_{5/2}) \rightarrow 3d^{10}4p\ (^2P°_{3/2})$, respectively.

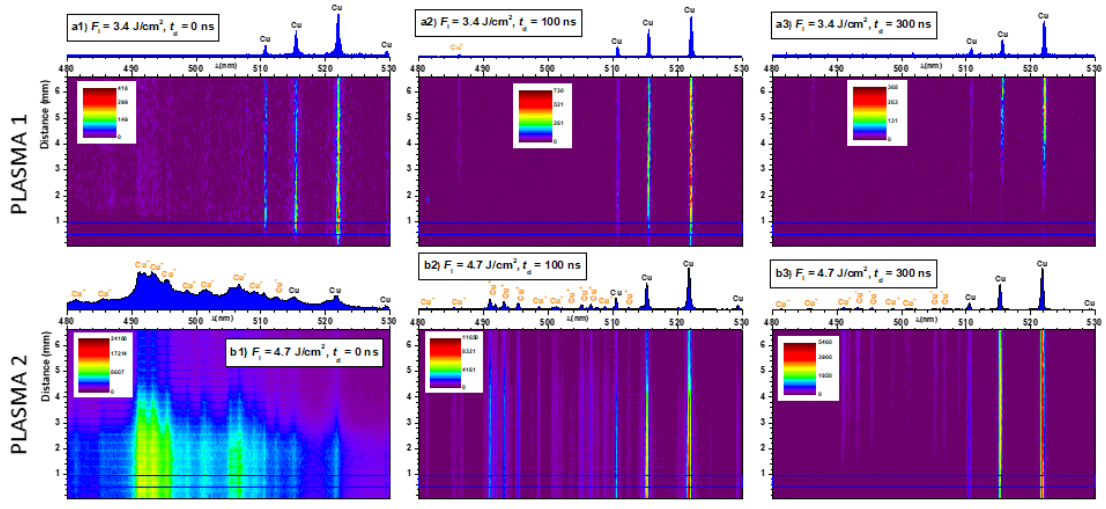

Figure 4. Spontaneous optical emissions from the Cu plasma, represented in 1D-1D maps as a function of wavelength (*x* axis) and distance from the target (*y* axis). Spectrally, the region chosen is 480-530 nm, which contains emissions from neutral Cu and Cu^+ ions. The top row (a1-a2-a3) contains the data for a 3.4 J/cm^2 ablation beam and the bottom row (b1-b2-b3), for a 4.7 J/cm^2 ablation beam. In all cases, emissions at the delays of 0 ns (left), 100 ns (middle) and 300 ns (right) with respect to the ablation event are shown. The horizontal lines on each map indicate the region of interaction with the driving beam in TH experiments.

Upon an increase of the laser ablation fluence from 3.4 J/cm^2 to 4.7 J/cm^2, the 1D-1D maps of OES emission change dramatically, as is displayed in the bottom row of **Figure 4**. This figure shows that immediately after ablation, continuum radiation dominates, due to the combination of Brehmsstrahlung processes (free-free transitions) and radiative recombination (free-bound transitions) [31], [40], [41]. This emission continuum shows superimposed Cu^+ and Cu lines. Shortly afterwards, the three neutral Cu emission lines at 510.55 nm, 515.32 nm and 521.82 nm described above become the most prominent contributions to the spectrum, but they are accompanied by a relatively intense plethora of ionic Cu^+ lines spreading from 481 to 513 nm. It is known that nanosecond lasers cause very significant ionization in laser plasmas, [42], [43] as opposed to shorter pulse (femtosecond) lasers, since the trailing part of the pulses can be absorbed by the plasma by reverse Bremsstrahlung and multiphoton absorption, causing additional excitation and ionization.

The series of space-integrated ($0 \leq z \leq 6.6$ mm) emission spectra as a function of time is shown in **Figure 5**, where the change for the dominant emission in the temporal region from 0 to 1 µs (continuum emission – Cu^+ ionic lines – Cu neutrals lines) can be better visualized. During the initial stages after the laser pulse ($t_d \leq 100$ ns), the continuum and Cu^+ emission dominate the spectra. The emission lines for Cu^+ progressively become spectrally narrower, as a consequence of the decrease in the electron density and electron temperature during plasma expansion. For longer delays ($t_d > 100$ ns), the intensity of Cu^+ emission lines steeply decreases as a consequence of the radiative recombination between these ions and electrons which is detected up to ≅ 500 ns.

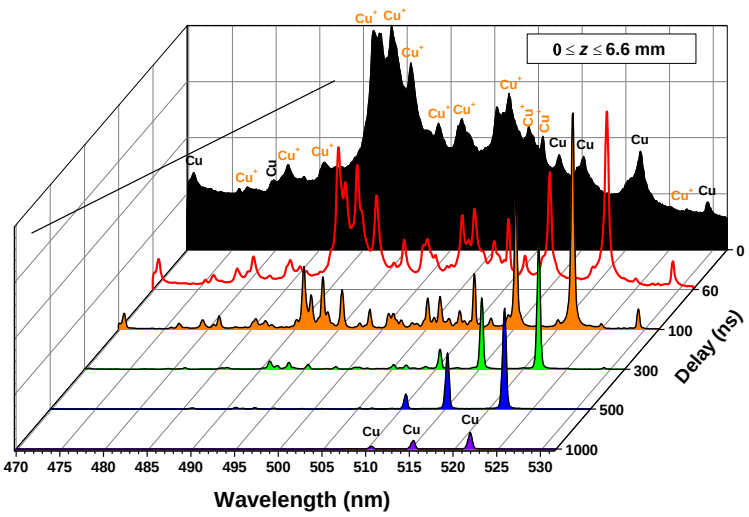

Figure 5. Spontaneous emission spectra from the Cu plasma as a function of time, acquired with a fixed gate width of 100 ns, for a 4.7 J/cm^2 ablation beam (*plasma 2*). The spectra correspond to spatially integrated emission maps over the $0 \leq z \leq 6.6$ mm range.

Another observation derived from the maps shown in **Figure 4** is that ionic emitters effectively move much faster away from the surface than neutrals. The expansion velocities of Cu and Cu^+ species were estimated from the evolution of the maxima of the vertical line-profiles as a function of the distance from the target, through a procedure analogous to that described in ref. [13]. Estimates of these effective velocities deduced from the neutral Cu emission at 521.82 nm ($3d^{10}4d\ ^2D_{5/2} \rightarrow 3d^{10}4p\ ^2P^0_{3/2}$) and Cu^+ at 495.37 nm ($3d^9(^2D_{3/2})\ 4f\ ^2[9/2]^0_5 \rightarrow 3d^9(^2D_{3/2})\ 4d\ ^2[7/2]_4$) yield an average speed of 10 ± 1 km/s for neutrals and 27 ± 2 km/s for singly ionized ions.

The detailed analysis of the optical emissions can provide estimations of the parameters defining the plasma, particularly electron density, ion stage distribution and local temperature [44], [13]. Atomic and ionic emission lines in plasmas are subject to the Stark effect due to collisions with electrons and ions. In laser-induced plasmas Stark broadening is normally the main broadening mechanism in comparison with Doppler or pressure broadening. Stark broadening contains the electron and ion broadening

components; for nonhydrogenic atoms electron impact is the predominant mechanism, so that the measurement of the Stark-broadened line profiles is a very powerful spectroscopic tool to obtain reasonable estimates of the electron density (n_e), through the expression[40]

$$\Delta\lambda_s = 2w\left(\frac{n_e}{n_{e,ref}}\right) \quad (1)$$

where $\Delta\lambda_S$ is the observed Stark broadening of the line (in Å), w is the electronic impact parameter and $n_{e,ref}$ is the electron density used as reference (often 10^{16} cm^{-3} for neutral atoms). For the Cu plasma we have selected the $3d^{10}\ 4p(^2P_{3/2}{}^0) \rightarrow 3d^{10}\ 4s(^2S_{1/2})$ line detected at 324.75 nm for which an accurate, relatively recent measurement has been found as reference [45]. This work tables a measured w of 12.5×10^{-3} nm at an electronic density of $n_e = 6.6\times10^{16}$ cm^{-3} and a plasma temperature of 19300 K. The spectral broadening observed in the present work in the spatiotemporal region of interest (1 mm from the surface, 300 ns after ablation) has been measured for *plasma 2* (4.7 J/cm^2) and a value of 0.15±0.05 nm (once deconvoluted from the instrumental width of 0.1 nm) has been obtained, which yields an electronic density in the range 8×10^{17} – 2×10^{18} cm^{-3}, assuming, as is normally the case, that the dependence of the impact parameter with temperature is slight [36]. For *plasma 1* (3.4 J/cm^2), the Stark spectral broadening is just below the detection threshold in our conditions, implying that the electron density in that case is $\leq 4\times10^{17}$ cm^{-3}.

Description of the plasma in terms of local temperature is only possible if the plasma is in or near a state of local thermodynamic equilibrium (LTE). The conditions for LTE have been discussed in detail by Fujimoto and McWhirter [46]. It is considered that LTE exists if the time between collisions is shorter than the other time scales relevant for plasma evolution. Therefore, high particle densities favor LTE. A necessary (albeit not sufficient [47]) requirement for the electron density can be formulated as follows [11]: n_e

(cm^{-3}) > 1.4×10^{14} $T_e^{1/2}$ $(\Delta E_{ul})^3$, where T_e is the electron temperature and ΔE_{ul} the separation between the upper and lower energy levels (both in eV). For the $3d^{10}\,4p(^2P_{3/2}{}^0)$ → $3d^{10}\,4s(^2S_{1/2})$ Cu transition observed at 324.75 nm, ΔE_{ul} = 3.8 eV. Since electron temperatures are expected to be in the region 1-2 eV (see below), in the most unfavorable case this threshold electron density would be 10^{16} cm^{-3}. Electron densities found in this work, which are in the region of 10^{17} – 10^{18} cm^{-3}, are sufficiently high so that LTE can be assumed.

With estimates of electron density and under LTE, the plasma emission spectra can be simulated by using the Saha-Boltzmann equations in combination with those that describe the intensity of spontaneous optical emissions. The Saha-Boltzmann system[40],[13] describes the ratio between the populations in different ionization stages:

$$\frac{N_{i+1}}{N_i} = \frac{2}{n_e}\frac{Z_{i+1}}{Z_i}\left(\frac{2\pi m_e\, kT}{h^2}\right)^{3/2} e^{-\varepsilon_i/kT}, \tag{2}$$

where N_i and N_{i+1} are the populations of the ionization stages i and i+1, respectively, Z_i and Z_{i+1} are the partition functions of these states, m_e is the electron mass, k is the Boltzmann constant, h is the Planck constant, n_e is the electron density and ε_i is the ionization energy. The system of Saha equations can be supplemented by the condition of electro-neutrality, $\sum i \times N_i = n_e$, where N_i is the density of species in the i-th state of ionization.

In a situation where self-absorption is not important, the intensity of a radiative transition from a given upper state u to a lower state l is given by [40]

$$I_{ul} = \frac{1}{4\pi} N_u A_{ul} \Delta E_{ul}, \tag{3}$$

where N_u is the population of the upper state, A_{ul} the Einstein coefficient for radiative spontaneous emission from the upper to the lower state, and ΔE_{ul} is the energy difference between the states.

We have carried out a simulation of the section of the spectra from 470 to 530 nm using the Saha–Boltzmann NIST code available online.[48] Some examples of simulations compared to the corresponding experimental spectra are displayed in **Figure 6**. The top and middle panels show the experimental spectra at the *plasma 1* (top panel) and *plasma 2* (middle panel), together with the best simulation for each case. Very good agreement can be achieved for both acquired spectra. For the simulations, an electron density of 4×10^{17} and 8.8×10^{17} cm^{-3} were chosen, respectively, for the case of moderate fluence shown in panel (a), and high fluence, shown in panel (b). Only small changes in the simulated spectra are observed for changes in the electron density value within the confidence range. On the other hand, changes in the plasma temperature do produce very significant modifications of the shape of the simulated spectra. The best fits were obtained for a plasma temperature of 0.9 eV for *plasma 1* and 1.3 eV for *plasma 2*. The relative intensity of the main three neutral Cu lines and the relative importance of the Cu^+ lines *versus* neutral lines are very sensitive indicators, so that the errors associated with these estimates are low, of the order of 5%. For a given electron density and plasma temperature, the Saha equations predict the ratio of the species with different degree of ionization. The values obtained are shown in **Figure 6(c)** for the whole range of temperatures from 0.4 eV to 2.0 eV, and for an electron density of 4×10^{17} cm^{-3} (displayed with open symbols and thin lines) and 8.8×10^{17} cm^{-3} (displayed with solid symbols and thick lines). On **Figure 6(c)**, two dashed vertical lines mark the temperature positions that provide the best fit to the two experimental situations studied. They indicate that Cu^+ ions are the predominant species in the plasma (90%) in *plasma 2* (4.7 J/cm^2, T=1.3 eV), whereas neutral Cu atoms constitute the majority of species (51%) for *plasma 1* (3.4 J/cm^2, T=0.9 eV).

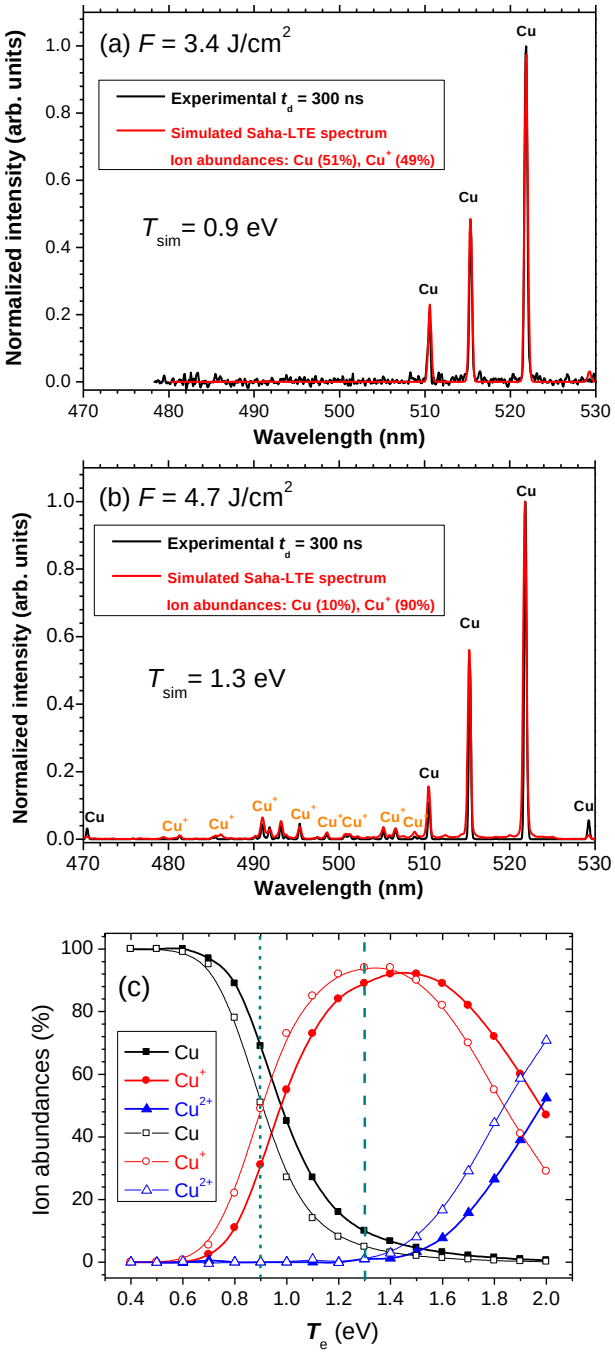

Figure 6. (a) and (b) Experimental and simulated emission spectra detected from the Cu plasma at 1 mm from the surface and 300 ns after ablation, for a fluence of (a) 3.4 J/cm^2 and (b) 4.7 J/cm^2. The simulations have been performed for the estimated electron densities at each laser fluence, i.e. 4×10^{17} cm^{-3} for (a) and 8.8×10^{17} cm^{-3} for (b). Best fit was achieved for a plasma temperature of 0.9 eV for the lower fluence (a) and 1.3 eV for the higher fluence (b). Estimates of proportions of Cu and Cu$^+$ species in both conditions are indicated on the panels. (c) Distribution of neutral and ionic Cu species in the plasma as a function of electron temperature as calculated with the Saha system of equations for an electron density of 8.8×10^{17} cm^{-3} (solid symbols, thick lines) and 4×10^{17} cm^{-3} (open symbols, thin lines). The two vertical dashed lines indicate the two temperature values that produce the best fit for the cases presented in panels (a) and (b).

4. Discussion

It is the comparison between the conditions of *plasma 1* and *plasma 2* that contains the key to the higher conversion efficiency for third harmonic generation for the former, and the significantly reduced efficiency for the latter. As has been noted before,[49] it is a complex combination of particle densities, phase matching and absorption, that determine optimum conditions for harmonic generation in a plasma.

We should first focus our attention to the microscopic aspect, i.e. the composition of the Cu plasma at the time and distance from the target where harmonics are produced. The analysis above shows that in *plasma 1* neutral Cu atoms are the major constituent (51%), whereas *plasma 2* is dominated by Cu^+ ions (90%). The densities of neutrals and ions in the plasma at the moment of arrival of the driving pulse define the microscopic generation efficiency, mediated by the third order nonlinear susceptibility of the two species at stake, Cu and Cu^+. It is known that ions can be the source of harmonic generation as well as neutrals, [28] but their nonlinear response is weaker [17]. However, this effect alone cannot account for the sharp efficiency drop beyond 3.5 J/cm^2. Even though the relative proportion of Cu atoms experiences a marked decrease for the higher fluence, the absolute density of neutral Cu atoms in the plasma is expected to be higher, which is confirmed through the measurement of the intensity of the spontaneous emission $3d^{10}\ 4p(^2P^0_{3/2}) \rightarrow 3d^{10}\ 4s(^2S_{1/2})$ at 324.75 nm, which grows by a factor of three from *plasma 1* to *plasma 2*.

Next, we will consider the macroscopic conditions for harmonic generation. In this respect, phase matching is the main concern, since harmonic generation only occurs efficiently if the harmonics emitted in different positions along the propagation direction interfere constructively, [50] which can only happen if the induced field is in phase with the driving field. As has been described in detail in the literature before, [51] the

contributors to dephasing are of two types: dispersion and geometrical. Both limit the coherence length, L_{coh}, i.e. the length over which the harmonic can be generated coherently in the medium.

The geometrical component of phase mismatch is also known as the Guoy phase shift, and is related to the π phase jump that a light beam experiences across its focus, of the form[52] $\varphi_{Guoy} = \arctan(2z/b)$, where b is the confocal parameter. However, for a finite medium that is short compared to the confocal parameter of the beam, only part of this phase shift occurs in the medium. The coherence length limited by this effect is given by $L_{coh}^{Guoy} = \pi b/2q$, where q is the harmonic order. This effect, thus, becomes important for high harmonic orders and tight focusing conditions. In the situation described in our experiments $L_{coh}^{Guoy} \approx 2$ mm. The length of the plasma medium used in the soft focusing geometry employed (spot size on the Cu target of 700 μm × 800 μm) is estimated to be approximately 1 mm. Since the Guoy phase shift is longer than the medium length, it can be considered that it does not limit phase matching in this case.

The second effect is related to the different group velocities of waves of different frequencies. The normal dispersion of atoms and ions can be disregarded in this experiment, since the atomic density is relatively low even for the conditions of *plasma 2* [53]. However, the presence of free electrons can have a considerable effect. The phase mismatch for the generation of harmonic q in the plasma due to the presence of free electrons is given by [54], [55]

$$\Delta k_{disp} = \frac{q\, n_e e^2 \lambda}{4\pi m_e \varepsilon_0 c^2} \tag{4}$$

where λ is the driving pulse wavelength, e and m_e are the electron charge and mass respectively, ε_0 is the permittivity of vacuum, c is the speed of light and n_e is the electron density.

This defines a coherence length L_{coh} in the medium over which the harmonic field and the polarization field stay in phase:

$$L_{coh} \approx \pi/\Delta k_{disp} \approx \frac{4\pi^2 m_e \varepsilon_0 c^2}{q\, n_e e^2 \lambda}. \quad (5)$$

For a driving field of 1064 nm wavelength this becomes

$$L_{coh}(mm) \approx \frac{1.05\times10^{18}}{q\, n_e(cm^{-3})}. \quad (6)$$

With the values estimated in this work for the electron densities, for *plasma 2* (8.8×10^{17} cm^{-3}), the expression above yields a coherence length of $L_{coh} \approx 0.4$ mm, whereas for *plasma 1* (4×10^{17} cm^{-3}), $L_{coh} \approx 0.9$ mm. Therefore, the coherence length is of the order of the length of the nonlinear medium for the moderate fluence employed, and significantly shorter than the medium for the higher fluence.

The output intensity of the generated harmonic in a medium of length L depends on the phase mismatch according to

$$I_q = I_q^{max} \frac{\sin^2(L\Delta k/2)}{(L\Delta k/2)^2}. \quad (7)$$

By introducing the estimates above, a drop of third harmonic generation by a factor of ten is expected for *plasma 2* in relation to *plasma 1* solely from the phase mismatch caused by free electrons. We can therefore conclude that this is the main factor limiting third harmonic generation above the optimum laser fluence value (≈ 3.4 J/cm^2) corresponding to the conditions of *plasma 1*. Finally, no significant absorption of the emitted third harmonic is expected, since there are no strong resonances of either Cu or Cu^+ in the vicinity of 355 nm [48].

The analysis above indicates that the fluence transition region from *plasma 1* to *plasma 2* corresponds to the transition from the dominance of neutral Cu atoms to Cu^+ ions. In correspondence with the presence of charged Cu^+ ions, a higher density of free electrons is present in the plasma, and it is the macroscopic detrimental effect of those on

phase matching that determines the reduced global efficiency of the plasma as a third order nonlinear medium.

It is interesting to point out that the sharp decrease of harmonic emission in a narrow ablation fluence window provides a method for the determination of electron densities in laser plasmas, in particular around the critical value for which the coherence length becomes of the order of length of the nonlinear plasma itself.

5. Conclusions

The characteristics defining NIR-laser ablation plasmas of Cu have been determined in this work, including ablation thresholds, ion abundances, expansion velocities, electron densities and electron temperatures. The study has focused on the impact of those characteristics on the properties of the laser plasma as an optical nonlinear medium, in particular for third-order harmonic generation. The micro- and macroscopic properties of the medium have been diagnosed through optical emission spectroscopy resolved in space and time, allowing for the direct characterization of the plasma region where harmonic generation is produced. An optimum ablation fluence window is detected in the region where the positive effect of increasing density is still not cancelled by the phase mismatch caused by free electrons.

Acknowledgements

This research was supported by the Spanish State Research Agency (AEI) and the European Regional Development (FEDER) through Projects CTQ2016-75880-P-AEI/FEDER, PID2019-106125GB-I00/AEI/10.13039/501100011033 and PID2019-104124RB-I00/AEI/10.13039/501100011033. M. O. thanks CSIC for contract.

References

[1] M. Stafe, A. Marcu, N.N. Puscas, Pulsed Laser Ablation of Solids, Springer, Berlin, Heidelberg, 2014. https://doi.org/https://doi.org/10.1007/978-3-642-40978-3.

[2] J.C. Miller, R.F.J. Haglund, Laser Ablation and Desorption, Academic Press, New York, 1997.

[3] M.N.R. Ashfold, F. Claeyssens, G.M. Fuge, S.J. Henley, Pulsed laser ablation and deposition of thin films, Chem. Soc. Rev. 33 (2004) 23–31. https://doi.org/10.1039/b207644f.

[4] A.K. Dubey, V. Yadava, Experimental study of Nd : YAG laser beam machining - An overview, J. Mater. Process. Technol. 195 (2008) 15–26. https://doi.org/10.1016/j.jmatprotec.2007.05.041.

[5] P.R. Willmott, J.R. Huber, Pulsed laser vaporization and deposition, Rev. Mod. Phys. 72 (2000) 315–328. https://doi.org/10.1103/RevModPhys.72.315.

[6] D.W. Hahn, N. Omenetto, Laser-Induced Breakdown Spectroscopy (LIBS), Part I: Review of Basic Diagnostics and Plasma-Particle Interactions: Still-Challenging Issues Within the Analytical Plasma Community, Appl. Spectrosc. 64 (2010) 335A-366A. https://doi.org/10.1366/000370210793561691.

[7] H. Tanaka, A. Matsumoto, K. Akinaga, A. Takahashi, T. Okada, Comparative study on emission characteristics of extreme ultraviolet radiation from CO2 and Nd : YAG laser-produced tin plasmas, Appl. Phys. Lett. 87 (2005) 041503. https://doi.org/10.1063/1.1989441.

[8] M.M. Murnane, H.C. Kapteyn, M.D. Rosen, R.W. Falcone, Ultrafast X-ray pulses from laser-produced plasmas, Science (80-.). 251 (1991) 531–536. https://doi.org/10.1126/science.251.4993.531.

[9] F. Caridi, L. Torrisi, L. Giuffrida, Time-of-flight and UV spectroscopy characterization of laser-generated plasma, Nucl. INSTRUMENTS METHODS Phys. Res. Sect. B-BEAM Interact. WITH Mater. ATOMS. 268 (2010) 499–505. https://doi.org/10.1016/j.nimb.2009.11.018.

[10] S.S. Harilal, C. V Bindhu, M.S. Tillack, F. Najmabadi, A.C. Gaeris, Internal structure and expansion dynamics of laser ablation plumes into ambient gases, J. Appl. Phys. 93 (2003) 2380–2388. https://doi.org/10.1063/1.1544070.

[11] S.S. Harilal, C. V Bindhu, R.C. Issac, V.P.N. Nampoori, C.P.G. Vallabhan, Electron density and temperature measurements in a laser produced carbon plasma, J. Appl. Phys. 82 (1997) 2140–2146. https://doi.org/10.1063/1.366276.

[12] C. Aragon, J.A. Aguilera, Characterization of laser induced plasmas by optical emission spectroscopy: A review of experiments and methods, Spectrochim. ACTA PART B-ATOMIC Spectrosc. 63 (2008) 893–916. https://doi.org/10.1016/j.sab.2008.05.010.

[13] J.J. Camacho, M. Oujja, M. Sanz, A. Martinez-Hernandez, I. Lopez-Quintas, R. de Nalda, M. Castillejo, Imaging spectroscopy of Ag plasmas produced by infrared nanosecond laser ablation, J. Anal. At. Spectrom. 34 (2019) 489–497. https://doi.org/10.1039/c8ja00353j.

[14] M. Oujja, R. de Nalda, M. Lopez-Arias, R. Torres, J.P. Marangos, M. Castillejo, CaF2 ablation plumes as a source of CaF molecules for harmonic generation, Phys. Rev. A. 81 (2010) 043841. https://doi.org/10.1103/PhysRevA.81.043841.

[15] R.A. Ganeev, M. Suzuki, M. Baba, H. Kuroda, T. Ozaki, Strong resonance enhancement of a single harmonic generated in the extreme ultraviolet range, Opt. Lett. 31 (2006) 1699–1701. https://doi.org/10.1364/OL.31.001699.

[16] R.A. Ganeev, L.B.E. Bom, J. Abdul-Hadi, M.C.H. Wong, J.P. Brichta, V.R. Bhardwaj, T. Ozaki, Higher-Order Harmonic Generation from Fullerene by Means of the Plasma Harmonic Method, Phys. Rev. Lett. 102 (2009) 013903. https://doi.org/10.1103/PhysRevLett.102.013903.

[17] R.A. Ganeev, Harmonic generation in laser-produced plasmas containing atoms, ions and clusters: a review, J. Mod. Opt. 59 (2012) 409–439. https://doi.org/10.1080/09500340.2011.636155.

[18] R. de Nalda, M. Lopez-Arias, M. Sanz, M. Oujja, M. Castillejo, Harmonic generation in ablation plasmas of wide bandgap semiconductors, Phys. Chem. Chem. Phys. 13 (2011) 10755–10761. https://doi.org/10.1039/c0cp02904a.

[19] M. Oujja, J.G. Izquierdo, L. Banares, R. de Nalda, M. Castillejo, Observation of middle-sized metal clusters in femtosecond laser ablation plasmas through nonlinear optics, Phys. Chem. Chem. Phys. 20 (2018) 16956–16965. https://doi.org/10.1039/c8cp02825g.

[20] R.A. Ganeev, M. Suzuki, M. Baba, M. Ichihara, H. Kuroda, High-order harmonic generation in Ag nanoparticle-containing plasma, J. Phys. B-ATOMIC Mol. Opt. Phys. 41 (2008) 045603. https://doi.org/10.1088/0953-4075/41/4/045603.

[21] M. Oujja, I. Lopez-Quintas, A. Benitez-Canete, R. de Nalda, M. Castillejo, Harmonic generation by atomic and nanoparticle precursors in a ZnS laser ablation plasma, Appl. Surf. Sci. 392 (2017) 572–580. https://doi.org/10.1016/j.apsusc.2016.09.087.

[22] I. Lopez-Quintas, M. Oujja, M. Sanz, M. Martin, R.A. Ganeev, M. Castillejo, Low-order harmonic generation in nanosecond laser ablation plasmas of carbon containing materials, Appl. Surf. Sci. 278 (2013) 33–37. https://doi.org/10.1016/j.apsusc.2012.10.105.

[23] M. Oujja, A. Benitez-Canete, M. Sanz, I. Lopez-Quintas, M. Martin, R. de Nalda, M. Castillejo, Frequency mixing in boron carbide laser ablation plasmas, Appl. Surf. Sci. 336 (2015) 53–58. https://doi.org/10.1016/j.apsusc.2014.09.119.

[24] L. Nagli, M. Gaft, Y. Raichlin, Third harmonic generation in double-pulse laser induced air plasma, Opt. Commun. 443 (2019) 63–68. https://doi.org/10.1016/j.optcom.2019.03.033.

[25] A.H. Sheinfux, Z. Henis, M. Levin, A. Zigler, Plasma structures for quasiphase matched high harmonic generation, Appl. Phys. Lett. 98 (2011) 141110. https://doi.org/10.1063/1.3578407.

[26] R.A. Ganeev, M. Suzuki, H. Kuroda, Quasi-phase-matching of high-order harmonics in multiple plasma jets, Phys. Rev. A. 89 (2014) 033821. https://doi.org/10.1103/PhysRevA.89.033821.

[27] J. Seres, V.S. Yakovlev, E. Seres, C. Streli, P. Wobrauschek, C. Spielmann, F. Krausz, Coherent superposition of laser-driven soft-X-ray harmonics from successive sources, Nat. Phys. 3 (2007) 878–883. https://doi.org/10.1038/nphys775.

[28] M. Suzuki, R.A. Ganeev, L.B.E. Bom, M. Baba, T. Ozaki, H. Kuroda, Extension of cutoff in high harmonic by using doubly charged ions in a laser-ablation plume, J. Opt. Soc. Am. B-OPTICAL Phys. 24 (2007) 2847–2852. https://doi.org/10.1364/JOSAB.24.002847.

[29] M. López-Arias, M. Oujja, M. Sanz, R.A. Ganeev, G.S. Boltaev, N.K. Satlikov, R.I. Tugushev, T. Usmanov, M. Castillejo, Low-order harmonic generation in metal ablation plasmas in nanosecond and picosecond laser regimes, J. Appl. Phys. 111 (2012). https://doi.org/10.1063/1.3686740.

[30] R.A. Ganeev, M. Suzuki, S. Yoneya, H. Kuroda, Electron density measurements using high-order harmonic generation in laser-produced plasmas, Appl. Phys. B-LASERS Opt. 121 (2015) 307–313. https://doi.org/10.1007/s00340-015-6230-x.

[31] A. De Giacomo, J. Hermann, Laser-induced plasma emission: From atomic to molecular spectra, J. Phys. D. Appl. Phys. 50 (2017) 183002. https://doi.org/10.1088/1361-6463/aa6585.

[32] M. Oujja, J.J. Camacho, M. Sanz, M. Castillejo, R. de Nalda, Optical diagnostics of gold plasmas produced by infrared laser ablation, J. Quant. Spectrosc. Radiat. Transf. 256 (2020) 107308. https://doi.org/https://doi.org/10.1016/j.jqsrt.2020.107308.

[33] R.J. Hendricks, D.M. Grant, P.F. Herskind, A. Dantan, M. Drewsen, An all-optical ion-loading technique for scalable microtrap architectures, Appl. Phys. B. 88 (2007) 507–513. https://doi.org/10.1007/s00340-007-2698-3.

[34] K. Sheridan, W. Lange, M. Keller, All-optical ion generation for ion trap loading, Appl. Phys. B. 104 (2011) 755. https://doi.org/10.1007/s00340-011-4563-7.

[35] D.A. Cremers, L.J. Radziemski, Handbook of laser-induced breakdown spectroscopy, 2nd Edition, Wiley, 2013.

[36] S. Amoruso, R. Bruzzese, N. Spinelli, R. Velotta, Characterization of laser-ablation plasmas, J. Phys. B-ATOMIC Mol. Opt. Phys. 32 (1999) R131–R172. https://doi.org/10.1088/0953-4075/32/14/201.

[37] L.M. Cabalin, J.J. Laserna, Experimental determination of laser induced breakdown thresholds of metals under nanosecond Q-switched laser operation, Spectrochim. ACTA PART B-ATOMIC Spectrosc. 53 (1998) 723–730. https://doi.org/10.1016/S0584-8547(98)00107-4.

[38] J.N. Agreda-Paredes, J.F. Agreda-Delgado, C.W. Aldama-Reyna, Pulsed photoacoustic determination of laser ablation threshold on metals, MOMENTO-REVISTA Fis. (2019) 49–65. https://doi.org/10.15446/mo.n59.75831.

[39] G.S. Boltaev, R.A. Ganeev, I.A. Kulagin, T. Usmanov, Resonance enhancement of the 11th harmonic of 1064 nm picosecond radiation generating in lead plasma, J. Opt. Soc. Am. B. 31 (2014) 436–442. https://doi.org/10.1364/JOSAB.31.000436.

[40] H.R. Griem, Principles of Plasma Spectroscopy, Cambridge University Press, 1997. https://doi.org/10.1017/CBO9780511524578.

[41] A. De Giacomo, R. Gaudiuso, M. Dell'Aglio, A. Santagata, The role of continuum radiation in laser induced plasma spectroscopy, Spectrochim. ACTA PART B-ATOMIC Spectrosc. 65 (2010) 385–394. https://doi.org/10.1016/j.sab.2010.03.016.

[42] O. Albert, S. Roger, Y. Glinec, J.C. Loulergue, J. Etchepare, C. Boulmer-Leborgne, J. Perriere, E. Millon, Time-resolved spectroscopy measurements of a titanium plasma induced by nanosecond and femtosecond lasers, Appl. Phys. A-MATERIALS Sci. Process. 76 (2003) 319–323. https://doi.org/10.1007/s00339-002-1815-8.

[43] J.R. Freeman, S.S. Harilal, P.K. Diwakar, B. Verhoff, A. Hassanein, Comparison of optical emission from nanosecond and femtosecond laser produced plasma in atmosphere and vacuum conditions, Spectrochim. ACTA PART B-ATOMIC Spectrosc. 87 (2013) 43–50. https://doi.org/10.1016/j.sab.2013.05.011.

[44] J.A. Aguilera, C. Aragon, Characterization of a laser-induced plasma by spatially resolved spectroscopy of neutral atom and ion emissions. Comparison of local and spatially integrated measurements, Spectrochim. ACTA PART B-ATOMIC Spectrosc. 59 (2004) 1861–1876. https://doi.org/10.1016/j.sab.2004.08.003.

[45] M. Burger, M. Skočić, Z. Nikolić, S. Bukvić, S. Djeniže, Broadening of the resonance Cu I lines in the laser-induced copper spectrum, J. Quant. Spectrosc. Radiat. Transf. 133 (2014) 589–595. https://doi.org/https://doi.org/10.1016/j.jqsrt.2013.09.022.

[46] T. Fujimoto, R.W.P. McWhirter, Validity criteria for local thermodynamic equilibrium in plasma spectroscopy, Phys. Rev. A. 42 (1990) 6588–6601. https://doi.org/10.1103/PhysRevA.42.6588.

[47] G. Cristoforetti, A. De Giacomo, M. Dell'Aglio, S. Legnaioli, E. Tognoni, V. Palleschi, N. Omenetto, Local Thermodynamic Equilibrium in Laser-Induced Breakdown Spectroscopy: Beyond the McWhirter criterion, Spectrochim. ACTA PART B-ATOMIC Spectrosc. 65 (2010) 86–95. https://doi.org/10.1016/j.sab.2009.11.005.

[48] A. Kramida, Y. Ralchenko, J. Reader, NIST ASD Team, NIST Atomic Spectra Database (version 5.7.1), Natl. Inst. Stand. Technol. Gaithersburg, MD. (2019). https://doi.org/https://doi.org/10.18434/T4W30F.

[49] R.A. Ganeev, M. Baba, M. Suzuki, H. Kuroda, High-order harmonic generation from silver plasma, Phys. Lett. A. 339 (2005) 103–109. https://doi.org/10.1016/j.physleta.2005.02.073.

[50] A. Lago, G. Hilber, R. Wallenstein, Optical-frequency conversion in gaseous media, Phys. Rev. A. 36 (1987) 3827–3836. https://doi.org/10.1103/PhysRevA.36.3827.

[51] H. Singhal, V. Arora, B.S. Rao, P.A. Naik, U. Chakravarty, R.A. Khan, P.D. Gupta, Dependence of high-order harmonic intensity on the length of preformed plasma plumes, Phys. Rev. A. 79 (2009) 23807. https://doi.org/10.1103/PhysRevA.79.023807.

[52] M.A. Porras, Characterization of the electric field of focused pulsed Gaussian beams for phase-sensitive interactions with matter, Opt. Lett. 34 (2009) 1546–1548. https://doi.org/10.1364/OL.34.001546.

[53] C.G. Wahlstrom, S. Borgstrom, J. Larsson, S.G. Pettersson, High-order harmonic generation in laser-produced ions using a near-infrared laser, Phys. Rev. A. 51 (1995) 585–591. https://doi.org/10.1103/PhysRevA.51.585.

[54] R.A. Ganeev, Frequency Conversion of Ultrashort Pulses in Extended Laser-Produced Plasmas, Springer Singapore, 2016. https://doi.org/10.1007/978-981-10-0194-9.

[55] F.J. Duarte, Laser Pulse Phenomena and Applications, InTechOpen, 2010. https://doi.org/10.5772/881.